THEMIS observations of magnetosheath-origin foreshock ions

Terry Z. Liu[1], Vassilis Angelopoulos[1], Andrew Vu[1], Hui Zhang[2], Antonius Otto[2], and Kun Zhang[3]

[1]Department of Earth, Planetary, and Space Sciences, University of California, Los Angeles, Los Angeles, CA, USA [2]Geophysical Institute, University of Alaska Fairbanks, Fairbanks, AK, USA [3]Space Science Institute, Boulder, CO, USA

Key points

1. Using observations of bow shock crossings by THEMIS, we investigate the magnetosheath-origin foreshock ions.

2. Foreshock ion density, velocity, phase space density, and distribution shape are consistent with non-adiabatic magnetosheath leakage.

3. Magnetosheath ion field-aligned anisotropy could cause leakage to become a dominant source of foreshock ions.

Abstract

The ion foreshock, filled with backstreaming foreshock ions, is very dynamic with many transient structures that disturb the bow shock and the magnetosphere-ionosphere system. It has been shown that foreshock ions can be generated through either solar wind reflection at the bow shock or leakage from the magnetosheath. While solar wind reflection is widely believed to be the dominant generation process, our investigation using THEMIS observations reveals that the relative importance of magnetosheath leakage has been underestimated. We show from case studies that when the magnetosheath ions exhibit field-aligned anisotropy, a large fraction of them attains sufficient field-aligned speed to escape upstream, resulting in very high foreshock ion

density. The observed foreshock ion density, velocity, phase space density, and distribution function shape are consistent with such an escape or leakage process. Our results suggest that magnetosheath leakage could be a significant contributor to the formation of the ion foreshock. Further characterization of the magnetosheath leakage process is a critical step towards building predictive models of the ion foreshock, a necessary step to better forecast foreshock-driven space weather effects.

1. Introduction

The ion foreshock is the region filled with backstreaming ions, upstream of the bow shock (see review by Eastwood et al., 2005). Because of the interaction between foreshock ions and solar wind ions, the ion foreshock is very dynamic and replete with many types of waves and transient structures (see review by Wilson, 2016; Zhang et al., 2022). These foreshock waves and foreshock transients can disturb the bow shock, magnetopause, and magnetosphere-ionosphere system. For example, they can drive magnetospheric ultra-low frequency waves, field-line resonances, and field-aligned currents that result in ionospheric traveling convection vortices and auroral brightening (e.g., Troitskaya et al., 1971; Sitar and Clauer, 1998; Fillingim et al., 2011; Eastwood et al., 2011; Hartinger et al., 2013; Wang B. et al., 2018, 2019, 2020, 2021; Liu et al., 2022a). However, these foreshock-driven disturbances are still not predictable. In order to forecast them, a predictive model of foreshock ions is necessary. To build such a model we need to first understand how the foreshock ions are generated.

The ion foreshock arises when the angle between the interplanetary magnetic field (IMF) and the bow shock normal, θ_{Bn}, is less than ~70° (see review by Burgess et al., 2012). One of the origins of foreshock ions is the solar wind reflection at the bow shock. Sonnerup (1969) derived the velocity of reflected solar wind ions at the bow shock in general situations. If the first adiabatic invariant is conserved, i.e., if reflection is adiabatic (e.g., Schwartz et al., 1983), the field-aligned solar wind ions in the de Hoffman Teller frame (HTF) reverse their parallel velocity at the shock. Transforming to the shock normal incidence frame (NIF) (around the bow shock nose, this would be close to the spacecraft rest frame), the solar wind ions gain two times the de Hoffman Teller (HT) velocity ($\boldsymbol{V_{HT}}$; the velocity of the HTF relative to the NIF) after the reflection. This energy gain in the NIF comes from gradient drift at the shock surface along the convection electric field, i.e., from shock drift acceleration (see review by Burgess et al., 2012).

Another origin of the foreshock ions is magnetosheath leakage (Edmiston et al., 1982). Due to the very large thermal speed of magnetosheath ions, some of them might be fast enough to escape upstream. In the leakage model by Edmiston et al. (1982), the first adiabatic invariant is assumed to be conserved, whereas in the model by Schwartz et al. (1983) leakage along the shock normal direction was also included. Schwartz and Burgess (1984) showed that both leakage and reflection mechanisms exist in observations. However, hybrid simulations and test particle simulations (e.g., Burgess and Luhmann, 1986; Burgess, 1987; Oka et al., 2005) showed that reflection is more likely the dominant origin.

In the models and simulations, the magnetosheath ions are considered to be isotropic or symmetric along the field-aligned direction. Using the Time History of Events and Macroscale Interactions during Substorms mission (THEMIS), we examine more than 500 bow shock crossings that are associated with foreshock ions. We show that the magnetosheath ions frequently exhibit field-aligned anisotropy towards the upstream direction which enhances the magnetosheath leakage. Thus, the role of magnetosheath leakage could have been underestimated. In Section 2, we introduce the THEMIS dataset. We present two case studies with and without field-aligned anisotropy and describe a non-adiabatic leakage process based on the observations in Section 3. We discuss our results in Section 4 and summarize in Section 5.

2. Data

We use data from the THEMIS mission (TH-A, TH-D, and TH-E spacecraft; Angelopoulos, 2008) while it was in fast survey mode (i.e., with distribution functions at maximum time resolution, ~3s) from 2016 to 2019. We analyze plasma data from electrostatic analyzer (ESA) (McFadden et al., 2008) and DC magnetic field data from fluxgate magnetometer (Auster et al., 2008). OMNI data is used for the pristine solar wind data. We calculate foreshock ion moments by removing solar wind ions from ion distribution functions by setting up a velocity radius around the solar wind (see detailed method in Liu et al. (2017)).

For each of ~500 bow shock crossings that are associated with foreshock ions (by examining the ion energy spectra), we manually select downstream time intervals (listed in the supporting information). To quantify the anisotropy of magnetosheath ions in the field-aligned direction, we calculate the heat flux along the field-aligned direction. We select two events for case studies in the next section, which have similar upstream parameters but very different magnetosheath anisotropy, leading to very different foreshock ion densities. Detailed statistical results can be found in the accompanying paper (Liu et al., 2023 submitted to JGR).

3. Results

3.1 Event 1

Figure 1 shows an overview of bow shock crossing by TH-D at [12.3, 2.2, 3.4] R_E in Geocentric Solar Ecliptic coordinates (GSE). The bow shock normal is [0.93, 0.17, 0.31] in GSE, calculated using the coplanarity method with both time-averaged magnetic field and velocity data

(Schwartz, 1998), which is consistent with [0.97, 0.13, 0.18] in GSE from the Merka et al. (2005) model. The Alfvén Mach number is quite large, ~19, due to the very low IMF strength (~2.5 nT) calculated using solar wind speed from OMNI (~350 km/s). In the later calculation, we ignore the bow shock normal velocity, because it was very small (~15 km/s earthward from conservation of mass flux (Schwartz, 1998)) compared to the foreshock ion velocity. Additionally, because the bow shock normal velocity was not constant and switched direction (the spacecraft crossed back into the magnetosheath ~10 min later, i.e., the spacecraft was close to the bow shock for a long period), the obtained velocity from one crossing cannot represent the entire time interval. Figures 1d and 1e show the parallel and anti-parallel energy flux of ions, those with pitch angles smaller than 80° and larger than 100°, respectively. Although the solar wind (the intense, narrow energy band flux at ~500eV in Figure 1e) was in the anti-parallel direction, the magnetosheath energy flux was overall stronger in the parallel direction. Upstream of the bow shock, the ions with energy higher than the solar wind ions were the foreshock ions (the broad energy band above 500 eV). Their energy flux was very close to that of the magnetosheath ions with high energy.

In this event, the bow shock was oblique with θ_{Bn} oscillating between 45° and 60° (Figure 2c). Corresponding to the θ_{Bn} oscillation, the foreshock ion density, velocity, and energy flux were also oscillating (Figures 2b, 2e-g). For the ions to stream upstream away from the bow shock, their parallel velocity projection along the bow-shock-normal component must be faster than this component of E×B velocity, i.e., $\boldsymbol{V}_{\parallel} \cdot \boldsymbol{n} + \boldsymbol{V}_{\boldsymbol{E}\times\boldsymbol{B}} \cdot \boldsymbol{n} > 0$. Figure 2d shows this minimum required parallel velocity in the spacecraft frame (nearly NIF). The oscillation of this minimum parallel velocity (caused by θ_{Bn} oscillation) can partially explain the observed foreshock ion velocity oscillation (Figure 2e). The observed foreshock ion parallel speed (Figure 2f) and foreshock ion density (Figure 2g) show very strong correlation (note that the parallel speed axis is reversed).

These results suggest a possibility that the foreshock ions could be leaked magnetosheath ions with parallel speed exceeding a threshold for leakage, such that a larger speed threshold due to a larger θ_{Bn} may cause fewer ions to escape.

To further investigate whether and how the leakage may have occurred, we analyze the ion distributions. Figures 3a and 3b show the magnetosheath ion distributions in the BV plane, where the horizontal axis is along the magnetic field and the plane contains the ion bulk velocity, and in the BE plane, where the plane contains the convection electric field instead. The distributions are averaged over the time interval corresponding to the orange shaded region in Figure 2 (also see similar ion distributions during other time intervals in Figure S1 in the supporting information). We chose 1-min time windows in order to smooth out the large field fluctuations. The magnetosheath ions show very strong anisotropy in the parallel direction, leading to parallel heat flux of $\sim 7.2 \times 10^{10}$ eV/cm^2/s (heat flux from 1-count noise is $\sim 1 \times 10^{9}$ eV/cm^2/s). This strong anisotropy is also seen from the parallel and anti-parallel energy spectra in Figure 1.

In the upstream region corresponding to the yellow shaded region in Figure 2, the foreshock ions were agyrotropic, and their parallel speeds depend on their gyrophases and pitch angles (Figures 3c and 3d). However, if we simply use the magnetosheath coordinates (identical to those in Figures 3a and 3b) to plot the foreshock ion distributions, the foreshock ions become quite "field-aligned" and "gyrotropic" (Figures 3e and 3f), with only a slight asymmetry. The shape and phase space density of the foreshock ion distributions were almost the same as the parallel population of the magnetosheath ions.

Such a comparison suggests a non-adiabatic leakage process. When some magnetosheath ions had field-aligned velocity projection along the bow-shock-normal component faster than this component of E×B velocity (vertical line #1 in Figure 3, average value from the orange shaded region), they can reach the bow shock and may be able to escape. Such a speed cutoff was consistent with the foreshock ion distributions in Figures 3e and 3f at small gyrovelocity. When these ions crossed the bow shock, their average motion direction only had a small change and was still roughly along the magnetosheath magnetic field rather than the IMF, causing partial gyration. Not all of them were able to stream far away from the bow shock, depending on their new gyrovelocity and parallel speed (vertical line #2 is from Figure 2d averaged over the yellow shaded region).

The reason why the leakage process is non-adiabatic is probably the very low field strength. Although the magnetosheath field strengths due to large-amplitude waves reached up to 20 nT (Figure 2a), the magnitude of average magnetic field vector $|\langle \boldsymbol{B} \rangle|$ was only ~5.1 nT, whereas the IMF strength was ~2.5 nT. As a result, the gyroradii of leaked ions can be 1000s of km when they crossed the bow shock, a large value compared to the shock thickness (100s of km).

To confirm the leakage more quantitatively, we calculate the partial density of magnetosheath ions which were faster than a speed threshold and compare it with the foreshock ion density. Ideally, we need to calculate the partial density beyond vertical line #1 in Figure 3a. However, because we do not have simultaneous magnetosheath observations to calculate this speed threshold, we use the parallel speed in Figure 2d as a proxy (corresponding to vertical line #2). (Theoretically, the two speed thresholds, in the spacecraft and NIF frame, can be calculated from $\boldsymbol{V}_{\boldsymbol{HT}}$ along the upstream and downstream magnetic field, but because the coplanarity of magnetic field was poorly satisfied, such a calculation cannot be used.) In Figure 2h, the calculated partial magnetosheath density from an averaged magnetosheath ion distribution shows a variability that is similar to the observed foreshock ion density (Figure 2g), and their magnitudes also roughly match. This similarity is consistent with the distribution function comparison in Figure 3 and further confirms the non-adiabatic leakage process.

Below we discuss some other processes that could happen during the leakage. For adiabatic leakage, magnetosheath ions perform magnetic gradient drift along the convection electric field and gain energy. In this event, however, the average motion of leaked ions changed only slightly across the bow shock indicating that such acceleration barely worked on average. For individual ions, on the other hand, the velocity direction can vary considerably across the bow shock. If the velocity direction variation in the HTF decreased (increased) the angle between the ion velocity and $\boldsymbol{V_{HT}}$, the ion energy increased (decreased) across the bow shock in the NIF. This means that the maximum possible speed of leaked ions in the NIF can be calculated by adding $\boldsymbol{V_{HT}}$ (~200-400 km/s) to the maximum magnetosheath ion speed in the HTF (~1000 km/s based on perpendicular speed in Figure 3b). Shown as the black line in Figure 2b, the energy corresponding to this maximum speed roughly matches the maximum energy of the ion spectrum.

Another important process is the cross-shock potential, which can accelerate leaked ions across the bow shock. The cross-shock potential is typically tens to several hundred Volts (e.g., Schwartz et al., 2021), which determines the minimum speed of leaked ions in the HTF (e.g., Schwartz et al., 1983). Based on the electron temperature increase across the bow shock (e.g., Schwartz et al., 1988), the cross-shock potential is estimated as ~20 V. Thus, its effect could be too weak to be seen for those keV ions.

The solar wind reflection and magnetosheath leakage are not necessarily exclusive. The vertical line #3 indicates the parallel speed of adiabatic reflection. It lies within the foreshock ion distributions, suggesting that the solar wind reflection might also contribute simultaneously.

Additionally, due to the very low field strength, it is also possible that the reflection process was non-adiabatic.

In summary, this case study suggests that due to the strong anisotropy of the magnetosheath ions in the parallel direction towards the upstream region, a large fraction of magnetosheath ions were moving fast enough to escape upstream, causing the ratio of foreshock ion density to solar wind density to be unusually high (more than 20%). After they leaked out, their average motion was still roughly following the magnetosheath field-aligned direction, meaning a non-adiabatic process likely due to the very low field strength and thus very large ion gyroradii.

The magnetosheath field-aligned anisotropy is not rare. Three more examples can be found in the supporting information (Figures S2-S4). In Figure S3, both the leakage population caused by the magnetosheath anisotropy and the diffuse foreshock population that traveled back to the magnetosheath can be seen. Likely related to the ion gyroradii, the leaked ions were more aligned with the IMF than with the magnetosheath field line in two examples (Figures S3 and S4), suggesting a more adiabatic process (the IMF strength was ~ 8 nT and 5 nT in these two cases, respectively). Statistical study in the accompanying paper (Liu et al., 2023 submitted to JGR) shows that most of events have field-aligned heat flux towards the upstream direction and ~56% of them are more than 5×10^{10} eV/cm^2/s. The possible causes of this anisotropy are discussed in Section 4.

3.2 Event 2

As a comparison, we present an example with isotropic magnetosheath ions, observed by TH-A at [11.9, -3.5, 4.9] R_E in GSE. The bow shock normal from the mixed-mode coplanarity method, [0.93, -0.19, 0.28] in GSE, is consistent with [0.95, -0.13, 0.27] in GSE from the Merka et al. (2015) model. Figures 4d and 4e show that the magnetosheath ion parallel and anti-parallel flux were similar, suggesting rather isotropic distributions (the parallel heat flux was only $\sim 1.6 \times 10^{10}$ eV/cm^2/s). Likely due to the isotropic distributions, there was weaker wave activity in this event compared to Event 1 and the average magnetic field on the two sides of the bow shock satisfied the coplanarity property much better than in Event 1. As shown in Figures 4a-c, the solar wind field strength, density, velocity, and the calculated Alfvén Mach number (~18) were all very close to those in Event 1. Although θ_{Bn} was also within 45° – 60° (Figure 5c) like in Event 1, the foreshock ion density (Figure 5g) was ~10 times smaller than that in Event 1. This indicates that the magnetosheath field-aligned anisotropy indeed significantly enhanced the foreshock ion density.

Without the anisotropy, the magnetosheath leakage would be weak but might still occur. Similar to Event 1, the calculated minimum parallel speed needed to stream away from the bow shock (Figure 5d) partially explains the observed foreshock ion velocity variation (Figure 5e). The observed foreshock ion parallel speed (Figure 5f) was correlated with the observed foreshock ion density (Figure 5g). The calculated partial magnetosheath density (Figure 5h), using the cutoff speed from Figure 5d, shows similar variation as the observed foreshock ion density. The calculated partial density overestimates the observed density because the cutoff speed from Figure 5d underestimates the magnetosheath escape speed (see vertical lines #1 and #2 in Figure 6).

Figure 6 compares the ion distributions in the magnetosheath and in the foreshock. Similarly, the foreshock ion distribution in the BE plane (Figures 6d and 6f) was more symmetric along the magnetosheath magnetic field than along the IMF. Additionally, the distribution in the BV plane (Figures 6c and 6e) was likely following a direction between the magnetosheath magnetic field and the IMF. This suggests the process was non-adiabatic but was closer to an adiabatic process than that in Event 1, probably due to the smaller ion gyroradii at the bow shock (although the IMF strength was similar, ~2.2 nT, the magnetosheath $|\langle \boldsymbol{B} \rangle|$ was ~10.1 nT). The maximum possible speed of leaked ions in the NIF was the maximum magnetosheath ion speed in the HTF (~900 km/s based on Figure 6b) plus $\boldsymbol{V_{HT}}$ (~300-500 km/s). Shown as the black line in Figure 5b, this maximum energy roughly matches the spectrum. These results suggest that the magnetosheath leakage might still contribute to the foreshock ions in this event, although much weaker than event 1.

The distribution function shape of foreshock ions was much more curved and broadened in the BE plane than in the BV plane, meaning very strong agyrotropy (Figures 6c and 6d). The magnetosheath ions were also more broadened along the convection electric field direction (Figure 6b) than along the E×B direction (Figure 6a). It is possible that due to their larger gyrovelocity in the BE plane, more magnetosheath ions on that plane can escape upstream than those in the BV plane. This preference likely amplified the agyrotropy of foreshock ions. Further work including simulations is needed to fully explain the distribution function shape beyond the qualitative analysis presented here.

The velocity of adiabatic reflection (vertical line #3) lies within the foreshock ion distributions. Because only a small fraction of magnetosheath ions is expected to leak out, the solar wind reflection could have a more significant impact than in Event 1. However, it is very difficult for observations to determine what is the relative contribution of reflection and leakage. Separating the two contributions in the future requires simulations.

3.3 Leakage process summary

We briefly summarize the magnetosheath leakage process (see sketch in Figure 7). In the HTF, the magnetosheath ion bulk velocity is along the magnetosheath field line, in the downstream direction (purple arrow). Due to their very large thermal speeds, some ions can have velocities directed upstream. When they cross the bow shock, they can be further accelerated by the cross-shock potential and scattered by the shock structures. Likely depending on the ion gyroradii at the bow shock relative to the shock thickness, the bulk motion of leaked ions (orange arrow) is between the magnetosheath field line direction ("fully" non-adiabatic) and IMF direction (adiabatic). Transforming to the NIF or spacecraft frame around the bow shock nose, the leaked ions can gain an additional field-aligned speed (and E×B speed) from $\boldsymbol{V_{HT}}$.

After the leakage, the leaked ions project their initial velocity along the IMF direction and become agyrotropic. As the magnetosheath field line direction is titled further away from the shock normal than the IMF direction, the projection from the magnetosheath field-aligned velocity into the perpendicular direction is always towards the bow shock. Due to this new gyrovelocity direction, the new field-aligned velocity has a minimum threshold for the leaked ions to stream away before they gyrate back to the bow shock (without gyrovelocity, this threshold is zero in the HTF). Additionally, depending on gyrophase, the projection from initial gyrovelocity can contribute negative field-aligned velocity, which could make the new field-aligned velocity towards the downstream direction. Thus, depending on their new gyrovelocity and field-aligned velocity in the upstream region, not all the leaked ions can stream far away from the bow shock along the IMF to contribute to the ion foreshock. For example, only the ions beyond at least the vertical line #2 in Figures 3c and 3d could stream far upstream. Thus, if there was a spacecraft further upstream (more than one foreshock ion gyroradius away), it would observe more field-aligned and more gyrotropic foreshock ions.

There is no reason for the magnetosheath leakage and solar wind reflection not to occur simultaneously. In the HTF, the maximum parallel speed of leaked ions is nearly the maximum speed of magnetosheath ions (and the minimum parallel speed is determined by the cross-shock potential), whereas the parallel speed of adiabatic reflection is the solar wind parallel speed in the HTF (green arrows), $V_{sw_{NIF}}/\cos\theta_{Bn}$ (Schwartz et al., 1983). For $\theta_{Bn} < 60°$, the adiabatic reflection speed ($< 2V_{sw_{NIF}}$) is very likely smaller than or comparable to the maximum magnetosheath ion speed in the HTF. At small θ_{Bn}, the reflected ions can become very diffuse, resulting in their bulk speed becoming comparable to the minimum parallel speed of the leaked ions. This means that the reflected ion contribution usually overlaps that of the leaked ions, and the two populations are very difficult to separate in observations. Nevertheless, when the magnetosheath ions exhibit strong field-aligned anisotropy towards the upstream, the leakage is expected to play a more important role.

The above considerations assumed a steady bow shock. When the bow shock is unstable and moves back-and-forth rapidly, the magnetosheath ions may not respond immediately. Assuming roughly the same magnetosheath ion distributions, under such rapid bow shock variations the relative speed between the magnetosheath ions and the bow shock also oscillates. Such oscillation could cause the magnetosheath ions to leak out more easily or less easily at the same periodicity.

4. Discussion

The field-aligned anisotropy of magnetosheath ions occurs frequently near the bow shock and has a strong preference towards the upstream direction. This means that there could be an ion source from further downstream. One possible source could be magnetospheric leakage (e.g., Anagnostopoulos et al., 1986, 2000; Sibeck et al., 1988). However, the IMF B_z was northward in Event 1, so at least magnetopause reconnection was unlikely. Another possible source arises as the field lines in the magnetosheath approach the magnetopause: they pile up and wrap around resulting in mirror force. Some of the fully heated magnetosheath ions could stream back towards the bow shock and mix with the newly heated magnetosheath ions leading to anisotropy. The case studies and statistical studies such as by Liu et al. (2023 submitted to JGR) support the latter possibility. Global hybrid simulations and multi-point observations could be conducted to further investigate the reason for the anisotropy in the future.

In order to forecast the foreshock-driven space weather effects, we need to establish predictive models of foreshock ions as a function of solar wind parameters. However, with almost the same shock parameters, the foreshock ion properties can be very different; this is how the two events are found. As discussed above, the cause of this difference is likely associated with the curved shape of the bow shock and magnetopause. Compared to ideal planar shocks, the downstream boundary of the sheath region, the magnetopause, could provide effects that propagate against the subsonic sheath flow towards the shock (e.g., local ion foreshock caused by a flux transfer event (Pfau-Kempf et al., 2016)). In other words, the simulations and theoretical models based on planar shocks could be insufficient to describe the Earth's bow shock and foreshock. More global models are needed.

When strong leakage occurs, the very high density of leaked ions could significantly modify the upstream conditions and strongly violate the MHD shock description. For example, the coplanarity of magnetic field across the bow shock in Event 1 was poorly satisfied. How to describe the shock jump conditions self-consistently under this situation is not trivial and requires future investigation.

5. Summary

Using THEMIS observations, we conduct two case studies to understand the origin of foreshock ions. We show that magnetosheath leakage could be a dominant source of foreshock ions when the magnetosheath ions exhibit strong field-aligned anisotropy in the upstream direction. The observations suggest a non-adiabatic leakage process in which the bulk motion of leaked ions deviates from the IMF direction, preferentially towards the magnetosheath field direction. Such a non-adiabatic process is likely caused by the very low field strength and thus the large ion gyroradii.

Our observations show that, due to the field-aligned anisotropy of magnetosheath ions, the foreshock ion density can be unusually large. Large foreshock ion density is a favorable condition for the occurrence and fast expansion of foreshock transients (Liu et al., 2022b, 2023; Vu et al., 2023). Therefore, the role of foreshock-driven perturbations (e.g., Wang B. et al., 2018, 2019) and particle acceleration (e.g., Liu et al., 2019; Turner et al., 2018) could have been underestimated by the use of planar shock models in prior investigations.

Acknowledgement

T. Z. L. is partially supported by NSF award AGS-1941012/2210319, NASA grant 80NSSC21K1437/80NSSC22K0791 and NASA grant 80NSSC23K0086. T. Z. L. and K. Z. acknowledge support by NSF award AGS-2247760. H. Z. is partially supported by NSF AGS-1352669. We acknowledge support by the NASA THEMIS contract NAS5-02099. We thank K. H. Glassmeier, U. Auster and W. Baumjohann for the use of the THEMIS/FGM data provided under the lead of the Technical University of Braunschweig and with financial support through the German Ministry for Economy and Technology and the German Center for Aviation and Space (DLR) under contract 50 OC 0302. We also thank the late C. W. Carlson and J. P. McFadden for use of THEMIS/ESA data. We also thank the SPEDAS team and the NASA Coordinated Data Analysis Web.

Data availability statement

THEMIS dataset are available at NASA's Coordinated Data Analysis Web (CDAWeb, http://cdaweb.gsfc.nasa.gov/). The SPEDAS software (see Angelopoulos et al. (2019)) is available at http://themis.ssl.berkeley.edu. The event list can be found in Table S1 in the supporting information.

Figures

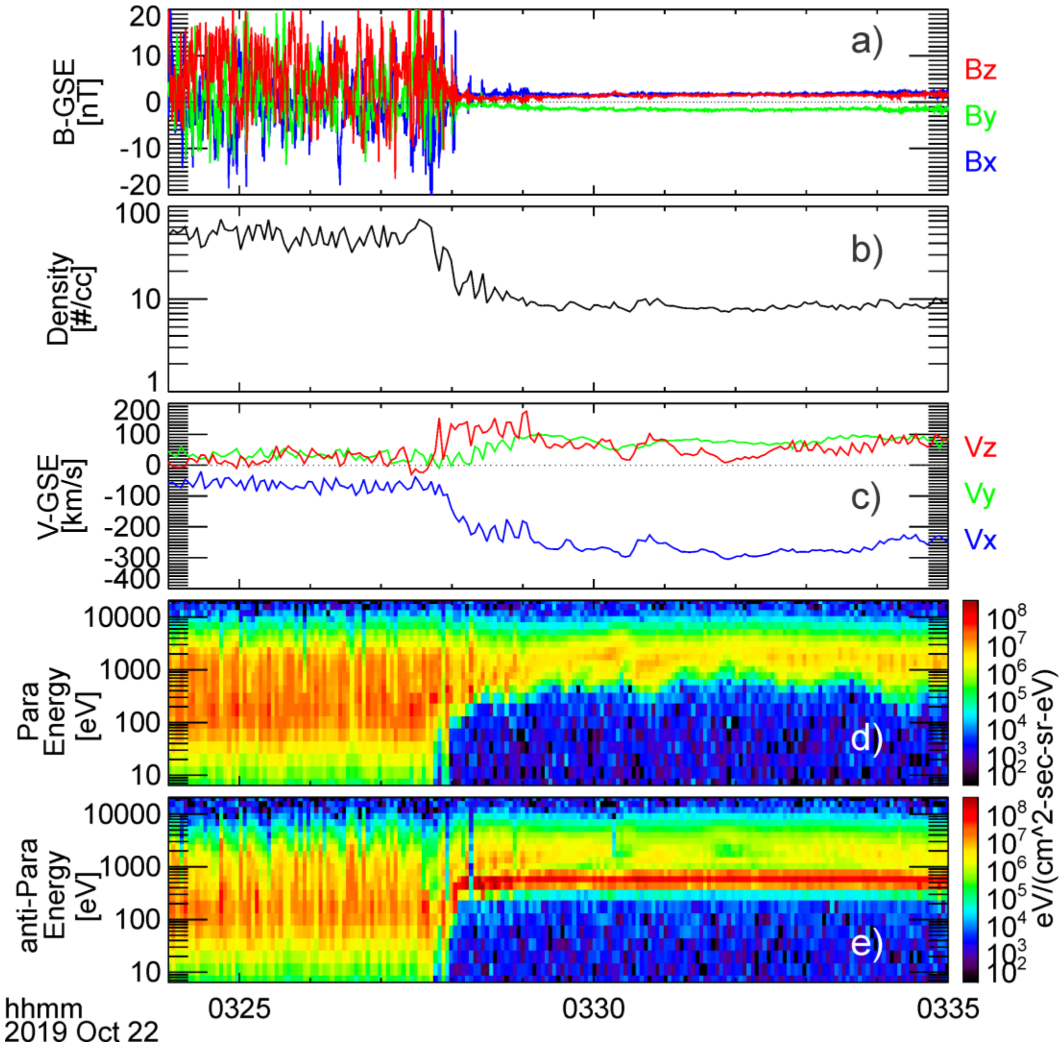

Figure 1. Overview plot of Event 1. From top to bottom: (a) magnetic field, (b) density, (c) ion bulk velocity, (d) ion parallel energy flux with pitch angle smaller than 80°, and (e) ion anti-parallel energy flux with pitch angle larger than 100°.

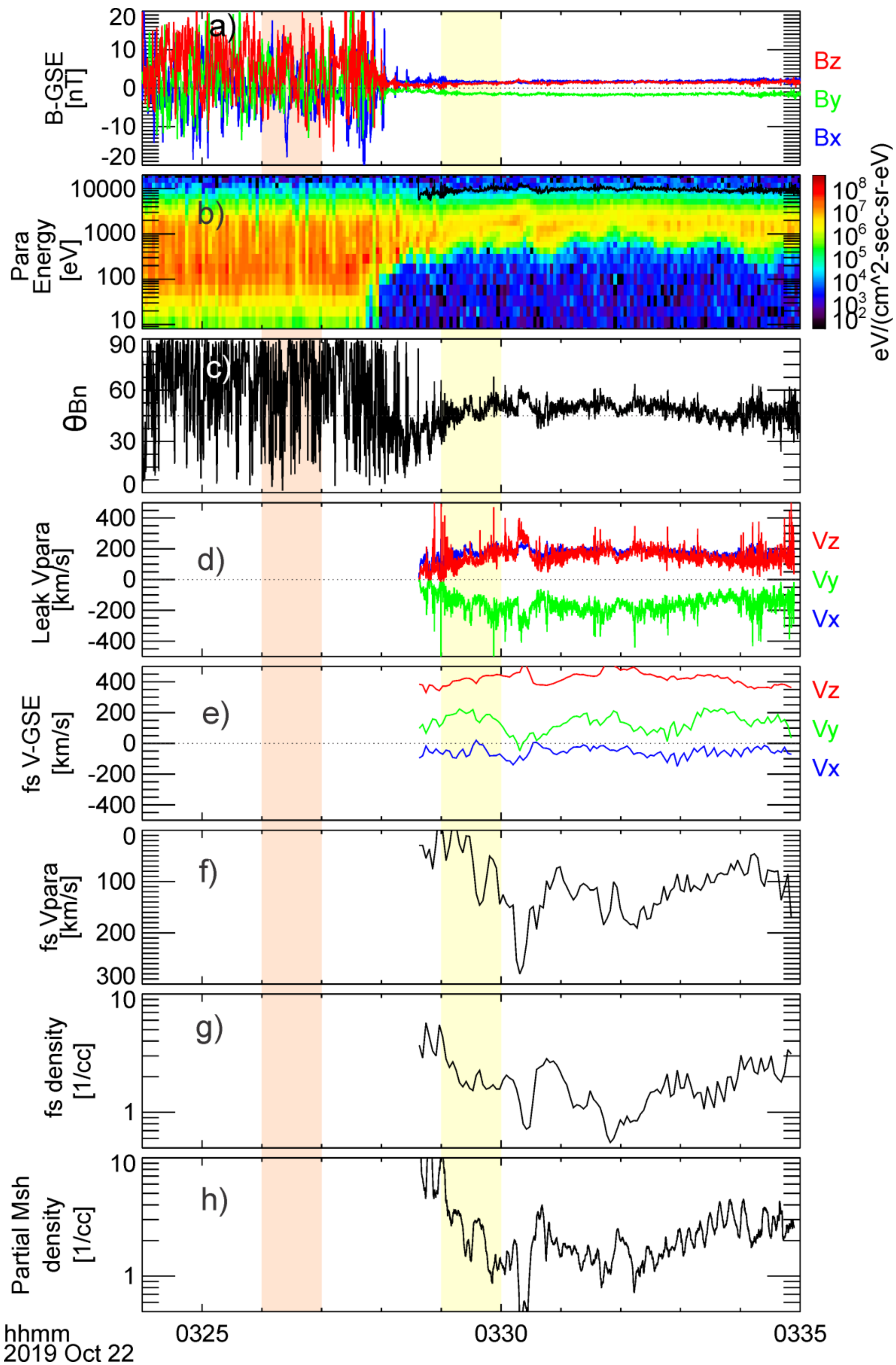

a)
B-GSE [nT]
Bz
By
Bx
b)
Para Energy [eV]
eV/(cm^2-sec-sr-eV)
c)
θBn
d)
Leak Vpara [km/s]
Vz
Vy
Vx
e)
fs V-GSE [km/s]
Vz
Vy
Vx
f)
fs Vpara [km/s]
g)
fs density [1/cc]
h)
Partial Msh density [1/cc]
hhmm
2019 Oct 22
0325
0330
0335

349

Figure 2. Continuation of Figure 1, showing derived products for Event 1. Panels (a) and (b) are repeats of panels (a) and (d) from Figure 1. For the rest panels from top to bottom: (c) θ_{Bn}, (d) the minimum parallel speed needed to stream away from the bow shock, (e) the observed foreshock ion bulk velocity, (f) the observed foreshock ion parallel speed (with vertical axis reversed), (g) the observed foreshock ion density, (h) the calculated partial density of magnetosheath ions with cutoff velocity from panel (d) and averaged ion distributions during 03:26:06 to 03:27:19 UT. The orange and yellow shaded regions indicate the time interval of ion distributions in Figure 3.

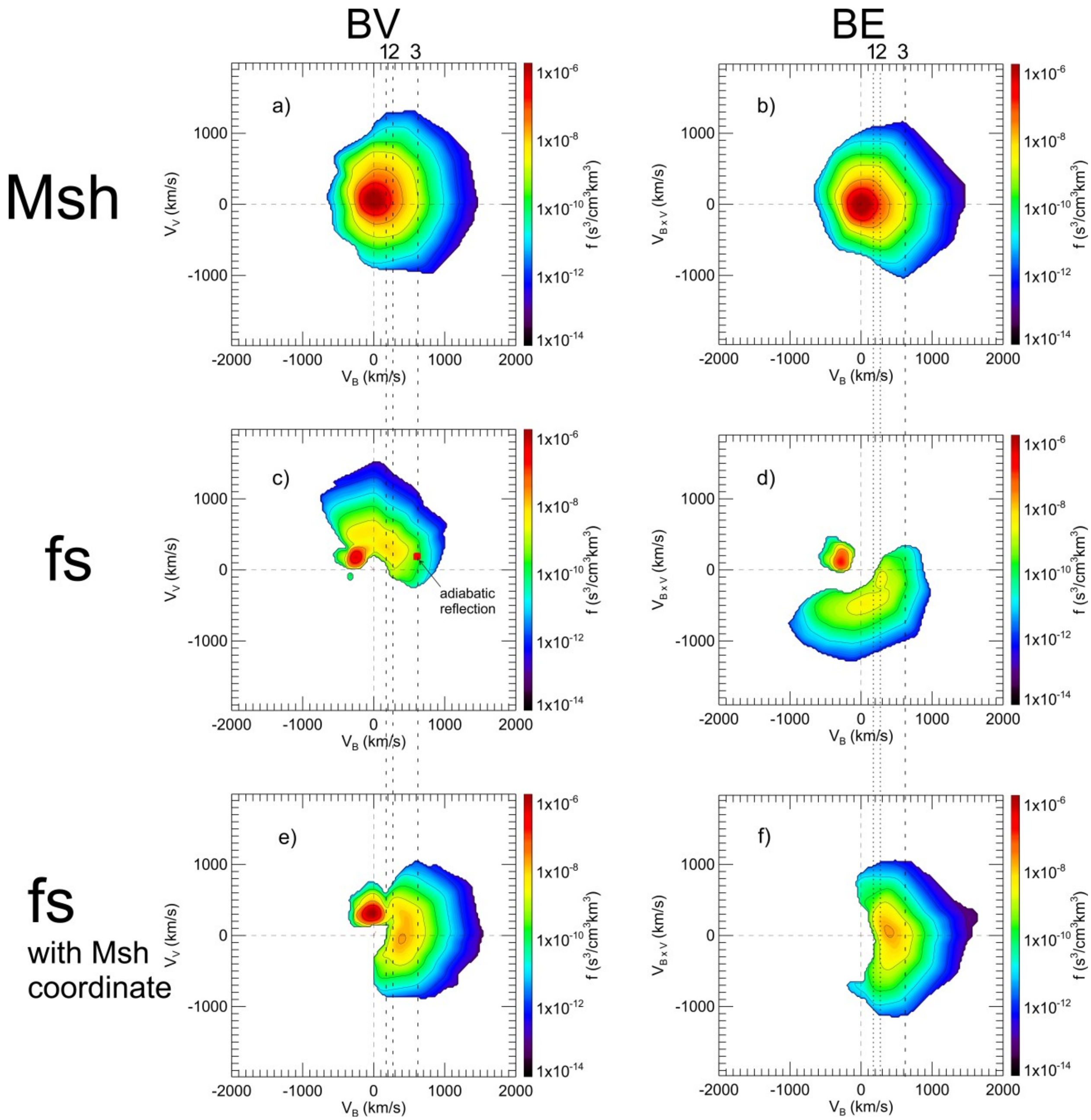

Figure 3. The ion distributions in the magnetosheath (Msh) and in the foreshock (fs) corresponding to the shaded regions in Figure 2. (a) Magnetosheath ion distribution in the BV plane where the horizontal axis is along the magnetic field and the plane contains the bulk velocity. (b) Magnetosheath ion distribution in the BE plane where the plane contains the convection electric field. (c) and (d) are the foreshock ion distributions in BV and BE planes. (e) and (f) are the same foreshock ion distributions but in the magnetosheath coordinates same as those in (a) and (b). The

vertical line #1 is the minimum magnetosheath parallel speed needed to reach the bow shock. The vertical line #2 is the minimum foreshock ion parallel speed needed to stream away from the bow shock. The vertical line #3 is the parallel speed of solar wind adiabatic reflection.

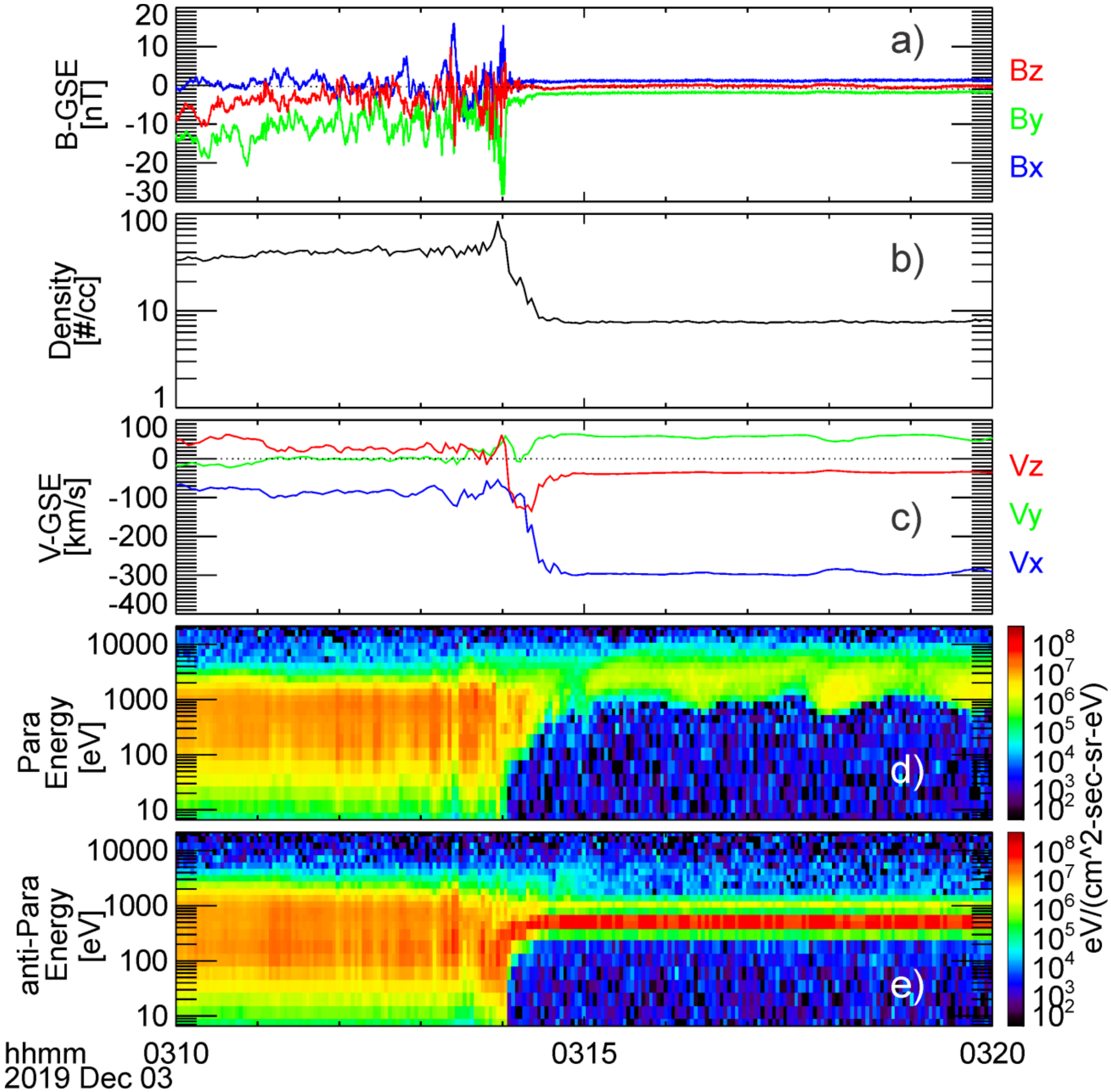

Figure 4. The overview of Event 2, same format as Figure 1.

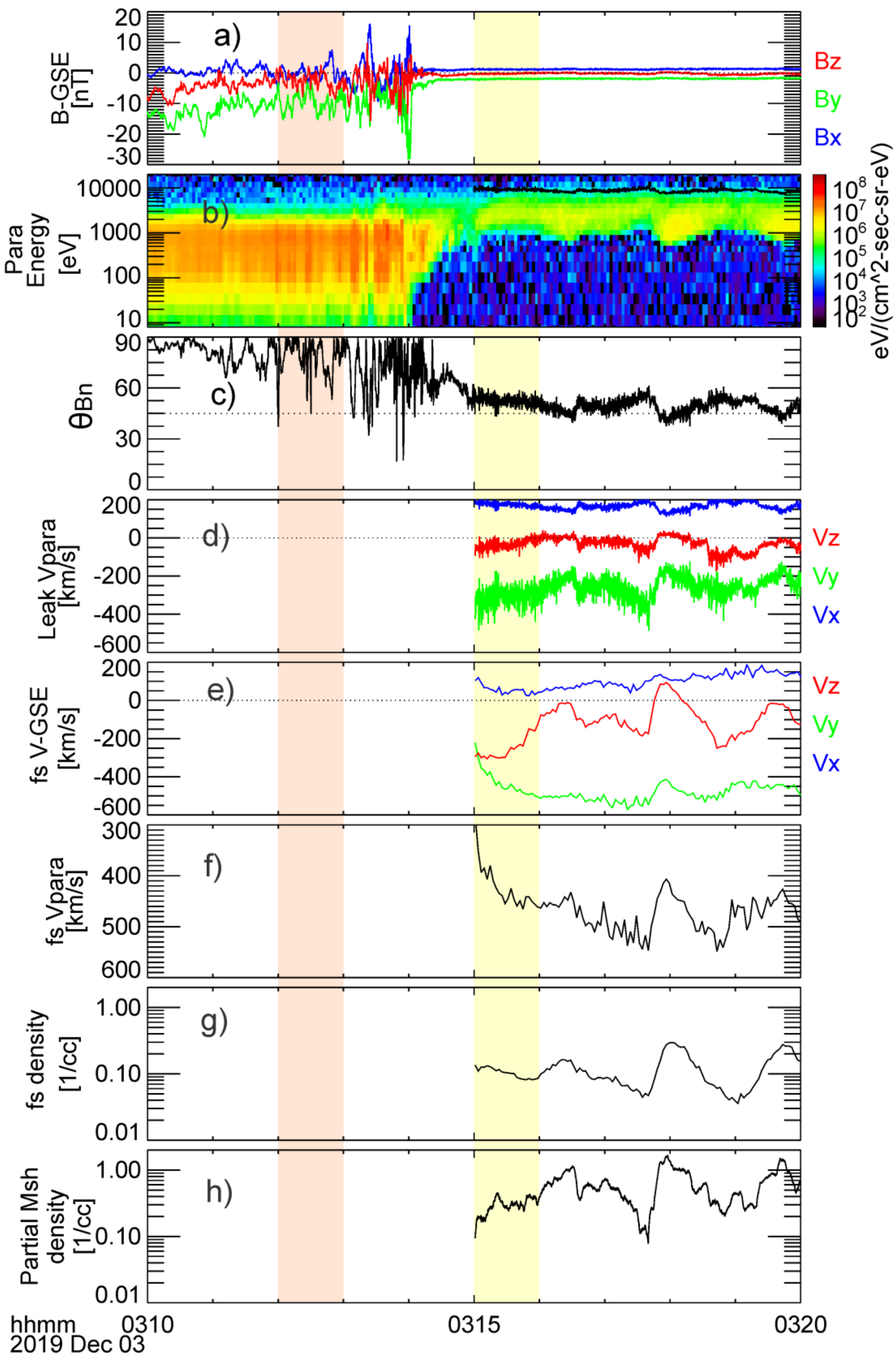

Figure 5. Continuation of Figure 4, showing derived products for Event 2, same format as Figure 2.

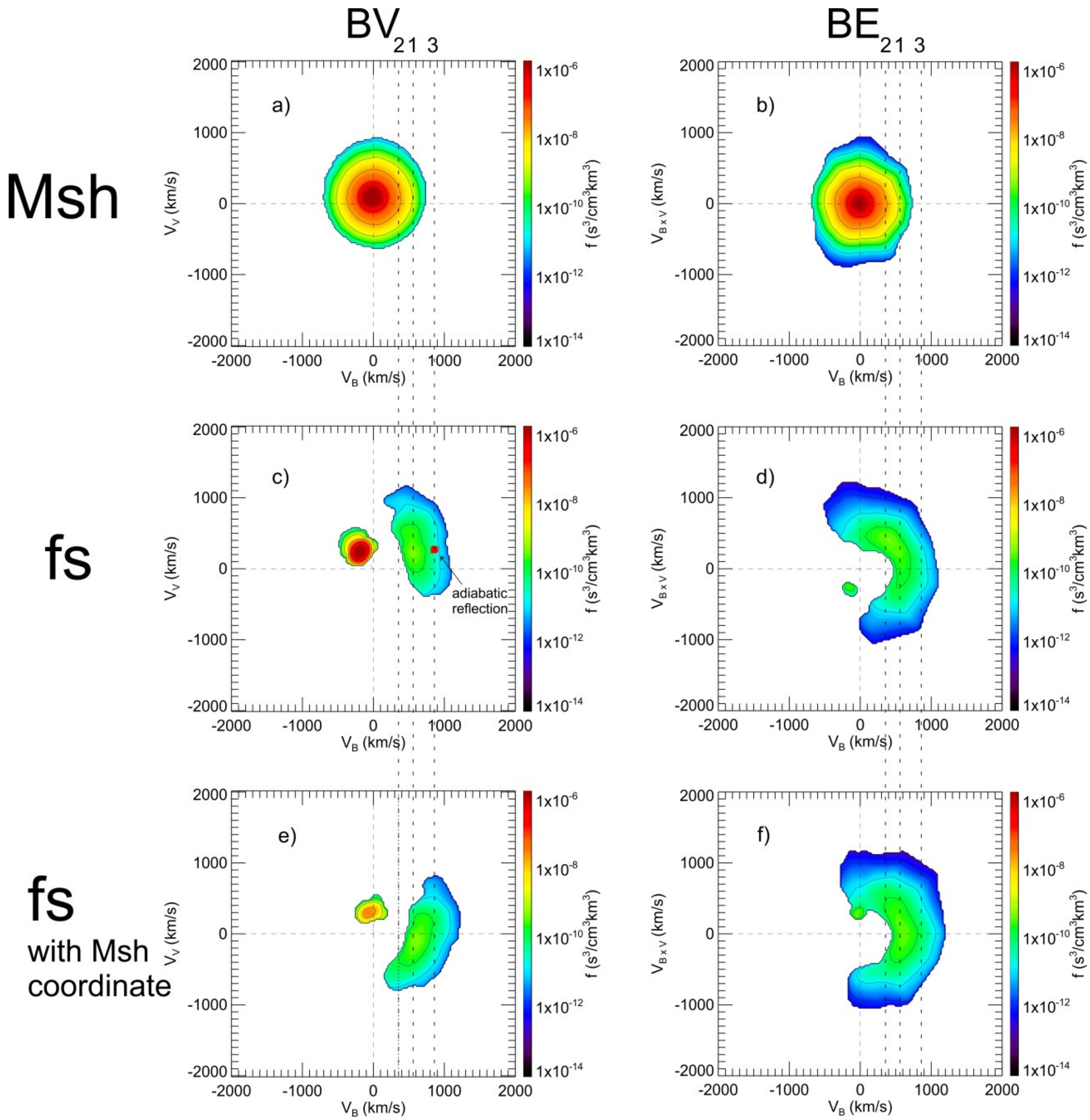

Figure 6. Ion distributions in Event 2, same format as Figure 3. Note that the minimum parallel speed for magnetosheath ions to reach the bow shock (vertical line #1) is larger than the minimum parallel speed for leaked ions to stream away from the bow shock (vertical line #2). This is different from event 1 because the coplanarity of magnetic field was poorly satisfied in Event 1.

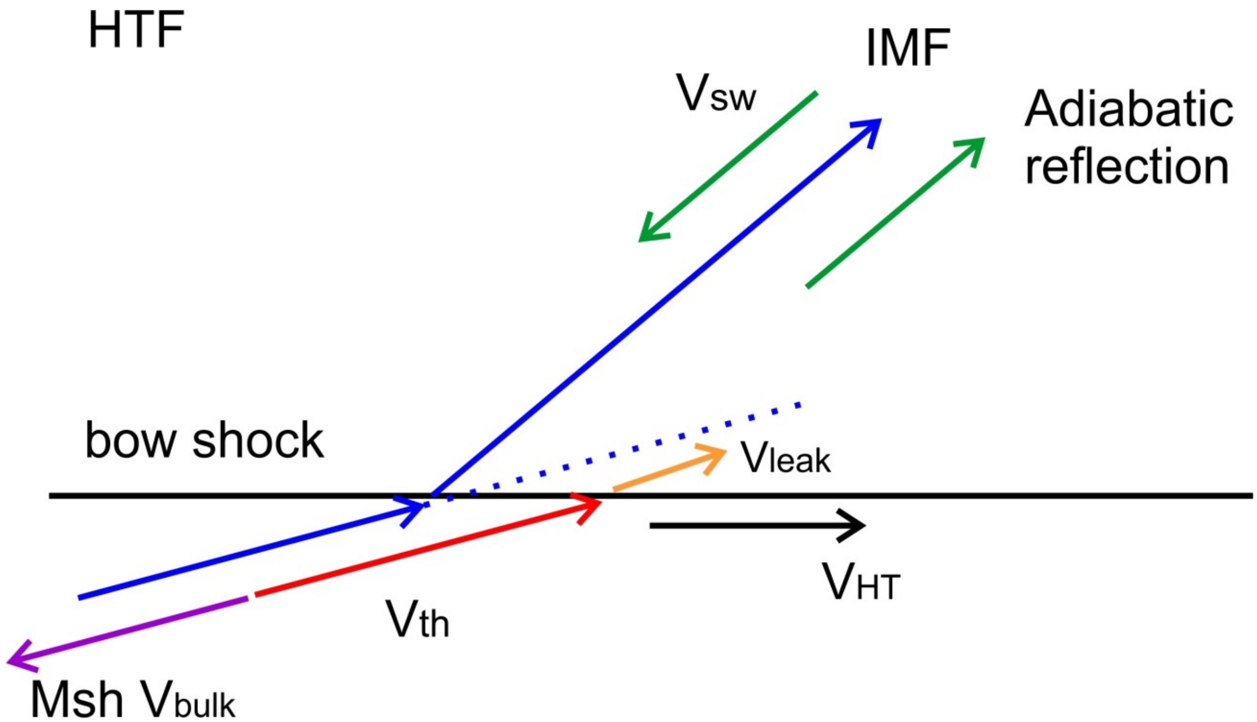

Figure 7. Sketch indicates the magnetosheath leakage process in the HTF. Magnetosheath ions with thermal speed (red arrows) outrunning the bulk velocity (purple arrows) can stream back to the solar wind by crossing the bow shock. After the crossing, depending on how non-adiabatic they are, the velocity of leaked ions (orange arrow) can be between the IMF and the magnetosheath field line (blue). Green lines indicate the solar wind velocity and the adiabatic reflection velocity.

References

Anagnostopoulos, G. C., N. Paschalidis, and A. N. Littas (2000), Energy time dispersion of a new class of magnetospheric ion events observed near the Earth's bow shock, Ann. Geophys., 18, 28–41, doi:10.1007/s00585-000-0028-8.

Anagnostopoulos, G. C., E. T. Sarris, and S. M. Krimigis (1986), Magnetospheric origin of energetic (E > 50 keV) ions upstream of the bow shock: The October 31, 1977, event, J. Geophys. Res., 91, 3020–3028.

Angelopoulos, V. (2008), The THEMIS mission, Space Sci. Rev., 141, 5–34, doi:10.1007/s11214-008-9336-1.

Angelopoulos, V., Cruce, P., Drozdov, A. et al. (2019). The Space Physics Environment Data Analysis System (SPEDAS) [Software]. Space Sci Rev 215: 9. https://doi.org/10.1007/s11214-018-0576-4

Burgess, D. (1987), Simulations of backstreaming ion beams formed at oblique shocks by direct reflection. Ann. Geophys. 5, 133–145 (1987)

Burgess D. and J.G. Luhmann (1986), Scatter-free propagation of low-energy protons in the magnetosheath—Implications for the production of field-aligned ion beams by nonthermal leakage. J. Geophys. Res. 91, 1439–1449. doi:10.1029/JA091iA02p01439

Burgess, D., Möbius, E. & Scholer, M. (2012). Ion Acceleration at the Earth’s Bow Shock. Space Sci Rev 173, 5–47. https://doi.org/10.1007/s11214-012-9901-5

Eastwood, J. P., E. A. Lucek, C. Mazelle, K. Meziane, Y. Narita, J. Pickett, and R. A. Treumann (2005), The Foreshock, Space. Sci. Rev., 118, 41–94, https://doi.org/10.1007/s11214-005-3824-3.

Eastwood, J., Schwartz, S., Horbury, T., Carr, C., Glassmeier, K.-H., Richter, I., et al. (2011). Transient Pc3 wave activity generated by a hot flow anomaly: Cluster, Rosetta, and ground-based observations. Journal of Geophysical Research, 116, A08224. https://doi.org/10.1029/2011JA016467

Edmiston, J.P., C.F. Kennel, D. Eichler, Escape of heated ions upstream of quasi-parallel shocks. Geophys. Res. Lett. 9, 531–534 (1982). doi:10.1029/GL009i005p00531

Hartinger, M. D., D. L. Turner, F. Plaschke, V. Angelopoulos, and H. Singer (2013), The role of transient ion foreshock phenomena in driving Pc5 ULF wave activity, J. Geophys. Res. Space Physics, 118, doi:10.1029/2012JA018349.

Liu, T. Z., Angelopoulos, V., Hietala, H., & Wilson, L. B. III (2017). Statistical study of particle acceleration in the core of foreshock transients. Journal of Geophysical Research: Space Physics, 122, 7197–7208. https://doi.org/10.1002/2017JA024043

Liu, T. Z., Angelopoulos, V., and Lu, S. (2019), Relativistic electrons generated at Earth's quasi-parallel bow shock, Science Advances, 5, 7, doi:10.1126/sciadv.aaw1368

Liu, T. Z., Wang, C.-P., Wang, X., Angelopoulos, V., Zhang, H., Lu, X., & Lin, Y. (2022a). Magnetospheric field-aligned current generation by foreshock transients: Contribution by flow vortices and pressure gradients. Journal of Geophysical Research: Space Physics, 127, e2022JA030700. https://doi.org/10.1029/2022JA030700

Liu, T. Z., Zhang, H., Turner, D., Vu, A., & Angelopoulos, V. (2022b). Statistical study of favorable foreshock ion properties for the formation of hot flow anomalies and foreshock bubbles. Journal of Geophysical Research: Space Physics, 127, e2022JA030273. https://doi.org/10.1029/2022JA030273

Liu, T. Z., Vu, A., Zhang, H., An, X., & Angelopoulos, V. (2023). Modeling the expansion speed of foreshock bubbles. Journal of Geophysical Research: Space Physics, 128, e2022JA030814. https://doi.org/10.1029/2022JA030814

Liu, T. Z., Angelopoulos, V, Zhang, H., Vu, A., and Raeder, J. (2023). Magnetosheath ion field-aligned anisotropy and implications for ion leakage to the foreshock, submitted to JGR

McFadden, J. P., C. W. Carlson, D. Larson, V. Angelopoulos, M. Ludlam, R. Abiad, B. Elliott, P. Turin, and M. Marckwordt (2008), The THEMIS ESA plasma instrument and in-flight calibration, Space Sci Rev., 141, 277–302, doi:10.1007/s11214-008-9440-2.

Merka, J., A. Szabo, J. A. Slavin, and M. Peredo (2005), Three-dimensional position and shape of the bow shock and their variation with upstream Mach numbers and interplanetary magnetic field orientation, J. Geophys. Res., 110 A04202, doi:10.1029/2004JA010944.

Oka, M., T. Terasawa, Y. Saito, T. Mukai, Field-aligned beam observations at the quasi-perpendicular bow shock: Generation and shock angle dependence. J. Geophys. Res. (Space Phys.) 110, 05101 (2005). doi:10.1029/2004JA010688

Pfau-Kempf, Y., H. Hietala, S.E. Milan, L. Juusola, S. Hoilijoki, U. Ganse, S. von Alfthan, M. Palmroth, Evidence for transient, local ion foreshocks caused by dayside magnetopause reconnection. Ann. Geophys. 34, 943–959 (2016). https://doi.org/10.5194/angeo-34-943-2016

Schwartz, S.J. and D. Burgess (1984), On the theoretical/observational comparison of field-aligned ion beams in the earth’s foreshock. J. Geophys. Res. 89, 2381–2384. doi:10.1029/JA089iA04p02381

Schwartz, S.J., M.F. Thomsen, J.T. Gosling (1983), Ions upstream of the earth's bow shock—A theoretical comparison of alternative source populations. J. Geophys. Res. 88, 2039–2047. doi:10.1029/JA088iA03p02039

Schwartz, S. J., Thomsen, M. F., Bame, S. J., and Stansberry, J. (1988), Electron heating and the potential jump across fast mode shocks, J. Geophys. Res., 93(A11), 12923– 12931, doi:10.1029/JA093iA11p12923.

Schwartz, S. J. (1998), Shock and discontinuity normal, Mach numbers, and related parameters, from Analysis Methods for Multi-Spacecraft Data, edited by G. Paschmann and P. W. Daly, pp. 249–270.

Schwartz, S. J., Ergun, R., Kucharek, H., Wilson, L., Chen, L.-J., Goodrich, K., et al. (2021). Evaluating the deHoffmann-Teller cross-shock potential at real collisionless shocks. Journal of Geophysical Research: Space Physics, 126, e2021JA029295. https://doi.org/10.1029/2021JA029295

Sibeck, D. G., R. W. McEntire, S. M. Krimigis, and D. N. Baker (1988), The magnetosphere as a sufficient source for upstream ions on November 1, 1984, J. Geophys. Res., 93, 14,328–14,342.

Sitar, R. J., and Clauer, C. R. (1999), Ground magnetic response to sudden changes in the interplanetary magnetic field orientation, J. Geophys. Res., 104(A12), 28343– 28350, doi:10.1029/1999JA900391.

Sonnerup, B.U.Ö. (1969), Acceleration of particles reflected at a shock front. J. Geophys. Res. 74, 1301–1304. doi:10.1029/JA074i005p01301

Troitskaya, V. A., T. A. Plyasova-Bakounina, and A. V. Gul'Elmi. The connection of Pc2–4 pulsations with the interplanetary magnetic field. Doklady Akademiia Nauk SSSR, 197:1312–1314 (1971)

Turner D. L. et al. (2018), Autogenous and efficient acceleration of energetic ions upstream of Earth's bow shock. Nature, 561, 206, doi:10.1038/s41586-018-0472-9

Vu, A., Liu, T. Z., Zhang, H., & Delamere, P. (2023). Parameter Dependencies of Early-Stage Tangential Discontinuity-Driven Foreshock Bubbles in Local Hybrid Simulations. Journal of Geophysical Research: Space Physics, 128, e2022JA030815. https://doi.org/10.1029/2022JA030815

Wang, B., Nishimura, Y., Hietala, H., Shen, X.-C., Shi, Q., Zhang, H., et 941 al. (2018). Dayside Magnetospheric and Ionospheric Responses to a Foreshock Transient on 25 June 2008: 2. 2-D Evolution Based on Dayside Auroral Imaging. Journal of Geophysical Research: Space Physics, 123(8), 6347–6359. https://doi.org/10.1029/2017JA024846

Wang, B., Nishimura, Y., Zhang, H., Shen, X.-C., Lyons, L., Angelopoulos, V., et al. (2019). The 2-D Structure of Foreshock-Driven Field Line Resonances Observed by THEMIS Satellite and Ground-Based Imager Conjunctions. Journal of Geophysical Research: Space Physics, 124(8), 6792–6811. https://doi.org/10.1029/2019JA026668

Wang, B., Liu, T., Nishimura, Y., Zhang, H., Hartinger, M., Shi, X., et al. (2020). Global propagation of magnetospheric Pc5 ULF waves driven by foreshock transients. Journal of Geophysical Research: Space Physics, 125, e2020JA028411. https://doi.org/10.1029/2020JA028411

Wang, B., Zhang, H., Liu, Z., Liu, T., Li, X., & Angelopoulos, V. (2021). Energy modulations of magnetospheric ions induced by foreshock transient-driven ultralow-frequency waves. Geophysical Research Letters, 48, e2021GL093913. https://doi.org/10.1029/2021GL093913

Wilson, L.B., III (2016). Low Frequency Waves at and Upstream of Collisionless Shocks. In Low-Frequency Waves in Space Plasmas (eds A. Keiling, D. - H. Lee and V. Nakariakov). doi:10.1002/9781119055006.ch16

Zhang, H., Zong, Q.-G., Connor, H. et al. Dayside transient phenomena and their impact on the magnetosphere and ionosphere. Space Sci Rev (2022). DOI: 10.1007/s11214-021-00865-0